Microchemical Journal 175 (2022) 107211

Contents lists available at ScienceDirect

Microchemical Journal

journal homepage: www.elsevier.com/locate/microc

Novel magnetic beads with improved performance for Alzheimer's disease biomarker detection

C. Toyos-Rodríguez [a,b], A. Llamedo-González [c,d], D. Pando [c], S. García [e], J.A. García [f], F. J. García-Alonso [b,d], A. de la Escosura-Muñiz [a,b,*]

[a] NanoBioAnalysis Group-Department of Physical and Analytical Chemistry, University of Oviedo, Julián Clavería 8, 33006 Oviedo, Spain
[b] Biotechnology Institute of Asturias, University of Oviedo, Santiago Gascon Building, 33006 Oviedo, Spain
[c] Nanovex Biotechnologies S.L., Parque Tecnológico de Asturias Edificio CEEI, 33428 Llanera, Spain
[d] NanoBioAnalysis Group-Department of Organic and Inorganic Chemistry, University of Oviedo, Julián Clavería 8, 33006 Oviedo, Spain
[e] Department of Psychology, University of Oviedo, Oviedo, Spain
[f] NanoBioAnalysis Group-Department of Physics, University of Oviedo, Calvo Sotelo s/n, 33007 Oviedo, Spain

ARTICLE INFO

Keywords:
Magnetic beads
Magnetic nanoparticles
Immunosensors
Alzheimer's disease
Electrochemical detection

ABSTRACT

Magnetic beads (MBs) have been notably used as platforms in biosensing thanks to their magnetic behavior as they allow to simplify purification and separation by preconcentrating the sample and also to minimize matrix effects, what facilitates the analysis of real samples. Even though it exists a variety of commercially available ones, there is still great interest to develop alternative MBs with improved performance. In this work, we propose the synthesis of novel, reliable and low-cost MBs by colloidal assembly of zinc doped magnetite for their use as electrochemical immunosensing platforms. First, zinc doped magnetite $Zn_xFe_{3-x}O_4$ nanoparticles (ZnFeNPs) of a diameter of 13 ± 3 nm and a saturation magnetization of 81 emu/g were synthesized and encapsulated in a polymeric matrix of poly(lactic-co-glycolic) acid (PLGA), generating polymeric MBs that were covered with polyethyleneimine (PEI) (MB@PEI), obtaining particles of 96 ± 16 nm. The PEI external layer provides MBs with a higher degree of encapsulation and stability and with functional groups that convert MB@PEI particles in versatile tools for their use as immunosensing platforms. In order to compare the suitability of the obtained MBs with commercially available ones, the affinity protein neutravidin (NAV) was linked to the MB@PEI surface through glutaraldehyde crosslinking. The obtained MB@NAV exhibited a significantly higher saturation magnetization than commercially available NAV-modified MBs, and also a better reproducibility (RSD of 4% for MB@NAV and 12% for commercial MBs) and enhanced surface functionalization ability when used as immunosensing platforms in a model assay using gold nanoparticle tags. As proof-of-concept of application in real samples, MB@NAV were finally applied for the detection of Tau protein, a well-known Alzheimer's Disease (AD) biomarker, with a detection limit (LOD) of 63 ng/mL and an excellent performance in human serum samples.

1. Introduction

Magnetic particles (MPs), those containing metals like iron or nickel as elements, oxides, or mixed oxides, have emerged as relevant materials in many different areas including bioimaging [1], drug delivery [2], wastewater treatment [3], biosensing [4,5] or in the isolation of complex matrices [6] among other applications.

MPs are typically used in the nanoscale range, from which superparamagnetic nanoparticles (SPIONs) are very appreciated by their stability and low toxicity [7]. In the nanoscale, the magnetic properties of these particles are size-dependent [8]. At lower diameters, lower than 20 nm, their saturation magnetization (Ms) increases with increasing particle size, regardless of particle shape. Up to 20 nm, the upper superparamagnetic limit [9] their remanent magnetization (Mr) starts to increase [10,11]. These SPIONs form stable liquid dispersions at room temperature [9] and exhibit high mobilities in the presence of external magnetic fields [12]. The most widely used route for the synthesis of SPIONs is the thermal decomposition of iron complexes as it generates high crystalline products with low polydispersity [13].

The reduced size of SPIONs entails, however, a low magnetic moment (m), what difficulties their functionalization without losing their magnetic behavior. An effective way to circumvent this difficulty is

* Corresponding author.
E-mail address: alfredo.escosura@uniovi.es (A. de la Escosura-Muñiz).

https://doi.org/10.1016/j.microc.2022.107211
Received 14 October 2021; Received in revised form 20 December 2021; Accepted 12 January 2022
Available online 19 January 2022

doping magnetite nanoparticles with Zn^{2+} ions, what enhances their magnetic properties, particularly its Ms, that increases significantly with the incorporation of a modest percentage of zinc(II) ions [14–16].

Another common way to increase magnetism is the encapsulation of magnetic nanoparticles into the so-called magnetic beads (MBs) that is, polymer spheres containing nanomagnetic particles randomly dispersed [17–19], thus the resulting material remains superparamagnetic but exhibits a fast response to external magnetic fields [20]. Accordingly, the employment of ZnFeNPs improves the magnetic moment of the MBs they are part of [21], taking advantage of both strategies.

There are a huge number of polymers that can be used to synthetize MBs, including poly(lactic-co-glycolic) acid (PLGA) [21–25]. PLGA is a biocompatible, biodegradable polymer widely used for encapsulation of different compounds for diagnosis in biomedicine as it is approved by the Food and Drug administration (FDA) and the European Medicines Agency (EMA) [26,27].

The use of MBs in immunosensing is extensive as they are interesting tools for the immobilization of biological recognition elements due to their high surface-to-volume ratio. As they can be moved by an external magnetic field, they allow the pre-concentration and separation of analytes of interest from complex samples, thus minimizing matrix effects [28–31]. Although the extensive use of commercially available MBs, there is still a great interest in obtaining alternative MBs for an improved performance [32,33].

Among the wide variety of analytes detected using MBs as immunosensing platforms, it is worthy to mention their application for the detection of Alzheimer's disease (AD) biomarkers [34–38]. AD is an untreatable and debilitating neurodegenerative disorder that affected more than 50 million people in 2019 and that is considered as the current main cause of dementia [39]. The diagnosis of AD is currently based on imaging techniques, mainly magnetic resonance imaging (MRI) for detecting abnormalities in patient brains [40] and the detection through immunohistochemistry and enzyme linked immunosorbent assay (ELISA) of cerebrospinal fluid (CSF) and blood plasma biomarkers [41].

Amyloid beta (Aβ) peptides plaques and hyperphosphorylated microtubule-associated protein Tau stand out from the biomarkers used for AD diagnostics. Tau protein is the main microtubule associated protein of the brain, that regulates axonal growth, transport or neuronal polarity through its phosphorylation. But, an hyperphosphorylation of this protein has been associated to the development of several neurodegenerative diseases, including AD [42–46].

In patients with AD, levels of Tau protein reach values of 195 pg/mL in cerebrospinal fluid (CSF) samples [47], although further research is needed to stablish reliable methodologies for sample acquisition and measurement that reduce the variability observed in the clinic between protein levels and the development of the disease [48,49].

In this work, ZnFeNPs with a high magnetization were synthesized following a thermal-decomposition procedure and used for the formation of MBs by encapsulation using PLGA as coating polymer. The obtained MB@PLGA were subsequently coated with polyethyleneimine (PEI) for increasing encapsulation and stability and providing the MBs with external functional groups for facilitating the ulterior bioconjugation of the affinity protein neutravidin (NAV) through glutaraldehyde crosslinking. The obtained MB@NAV were used as immunosensing platforms in a model immunoassay using gold nanoparticles (AuNPs) as labels, proving their suitability in immunosensing. Their performance was compared with that of commercially available MBs, showing comparable results with an increased reproducibility (RSD of 4% vs 12%) and an enhanced surface functionalization ability for the immobilization of specific antibodies. As proof-of-concept of application in real samples, MB@NAV were also implemented for the detection of Tau protein with a LOD of 63 ng/mL and a good performance in human serum samples.

2. Experimental

2.1. Reagents and materials

Benzyl ether 98%, glutaraldehyde solution grade II 25%, iron (III) acetylacetonate 97%, neutravidin, oleic acid 90%, polyethylenimine, branched Mw ~ 25.000, poly(lactic-co-glycolic acid) (PLGA) Resomer® RG 503H 50:50, polyvinyl alcohol (PVA) 31.000–50.000 wt 87–89% hydrolyzed, albumin, from bovine serum (BSA), anti-Human IgG (γ-chain specific)-Biotin, gold (III) chloride trihydrate 99.9%, Human IgG greater than 95% (HPLC grade), anti-Tau antibody, clone 12, from mouse and Tau-441 protein were purchased from Sigma-Aldrich (Spain). Zinc (II) acetylacetonate 95%, 2-propanol hyper grad LiChrosol®, tri-sodium citrate trihydrate and Tween-20 detergent were obtained from Merk Millipore (Spain). Petroleum ether 40/60, streptavidin-modified magnetic beads (M−280) and biotinylated Tau monoclonal antibody (BT2) were purchased from Thermo Fisher Scientific (Spain). Dichloromethane anhydrous (0.001% water) was obtained from VWR International Eurolabs (Spain) and oleylamine (approximate C-18 content 80–90%) was obtained from Acros Organics (Spain). Polyclonal rabbit anti-mouse immunoglobulin (used as control) was purchased from Dako Products /Agilent (USA).

Solutions were prepared, unless otherwise stated, using ultrapure water (18.2 MΩ·cm @ 25 °C) taken from a Millipore Direct-Q 3 UV purification system purchased from Millipore Ibérica S.A. (Spain). Phosphate buffer electrolyte solution was prepared using as precursors sodium chloride, potassium chloride, disodium hydrogen phosphate and potassium dihydrogen phosphate all obtained from Merck (Germany). Two different buffers were used in the MB bioconjugation process: a binding and washing (B&W) buffer composed of 0.1 M PBS pH 7.2 solution with 0.05% (v/v) Tween-20 and a blocking buffer (BB) consisted in 0.1 M PBS pH 7.2 solution with 5% (w/v) BSA.

2.2. Instrumentation

A transmission electron microscopy (TEM), either a JEOL JEM 2100 HRTEM and a JEOL2000 EXII TEM were used for size characterization of the as-synthesized nanoparticles. Size distribution was obtained by measuring the diameter of each particle with ImageJ software. Dynamic light scattering (DLS) was also performed using a Malvern Instruments Zetasizer Nano SZ with a solid-state He–Ne laser (wavelength $\lambda = 633$ nm).

X-ray powder diffraction (XRPD) was used to obtain the composition profile of the ZnFeNPs and the crystallinity size of the particles, using CuKα1,2 radiation ($\lambda = 1{:}54056$ Å and 1.54439 Å) in a Bragg-Brentano reflection configuration, on a PHILIPS X' PERT PRO Panalytical diffractometer in a 2θ range of 15–90°, with a step size of 0.03 using bulk magnetite as comparison. Infrared spectroscopy (IR) was performed using a Fourier transform infrared spectroscopic (FTIR) Spectrometer Paragon 1000 from PerkinElmer (USA) using KBr pressed disks.

Inductively coupled plasma mass spectrometry (ICP-MS) analysis was done using a Triple Quad 8800 ICP-QQQ from Agilent equipped with a concentric nebulizer with double-class glassy spray chamber to correlate the composition of zinc present in the nanoparticles. Additionally, magnetic measurements were performed at room temperature using a PPMS-14 T (Physical Property Measurement System).

A rotary evaporator IKA® RV8, from VWR International, was used for the MBs synthesis. A MagRack® 6 provided by Sigma-Aldrich (Spain) was used for magnetic separation processes. A MSC-100 cooling thermo shaker from Labolan (Spain) was used for the immunoassay incubations. Purification of AuNPs before and after bioconjugation with antibodies was done using a thermostatic centrifuge (Rotanta 460 R) from Hettich (Germany).

Electrochemical measurements were done using a μAutolab type II controlled by Autolab GPES software from Metrohm (Switzerland). Screen-printed carbon electrodes (SPCEs, ref DRP-110) and their

connector to the potentiostat (ref. DRP-DSC) were obtained from Metrohm DropSens S.L. (Spain). The SPCEs have a conventional three-electrode configuration including a working and counter electrode both composed of carbon and a silver pseudoreference electrode. A magnetic support for SPEs (DRP-MAGNET-700) purchased from Metrohm DropSens S.L. (Spain) was used for the electrochemical measurements with the MBs.

2.3. Synthesis and characterization of ZnFeNPs

ZnFeNPs were synthesized following a previously published procedure [50] with slight modifications. For the synthesis, 4 mmol Fe $(acac)_3$ and 0.68 mmol $Zn(acac)_2$ were dispersed in a mixture of 20 mL dibenzyl ether, 2.8 mL oleylamine and 2.7 mL oleic acid previously deoxygenated by purging Ar for 30 min. The mixture was placed in a three-necked round-bottom flask and heated with vigorous mechanical stirring, refrigeration, and inert atmosphere until reflux. When reflux was achieved, the reaction was maintained for 15 min under the same conditions. Afterwards, heating was removed, and the reaction was maintained at vigorous stirring for 15 min more, completing the first heating step. Then, a second heating step was performed by reconnecting the heating source and maintaining the reaction under reflux for 2 h. After this time, heating was removed again, and the reaction was maintained under stirring for 30 min, when it was separated and let it cool down. The obtained particles were purified by washing with a mixture 1:1 in volume of 2-propanol and light petroleum ether using an external magnetic disk and dried under vacuum. Dried particles were reconstituted in 2-propanol at a concentration of ~ 100 mg/mL.

The obtained NPs were characterized through TEM, XRDP, IR, ICP and magnetic measurement of the room temperature hysteresis loops.

2.4. Synthesis and characterization of magnetic beads (MBs)

MBs were synthesized following a water in oil emulsion procedure. First, 1.0 mL of ZnFeNPs suspension in 2-propanol was added to 2.0 mL of a 25 mg/mL PLGA solution in dimethylformamide (DMF) in a 15 mL centrifuge tube and vortexed for 15 s. The mixture was then transferred to a 50 mL centrifuge tube containing 15 mL of PVA 2% solution and then vortexed for 30 s and homogenized using a Branson® digital sonifier S450D during 1 min in pulses of 1 s (30 pulses/min) at a 65% amplitude. The PLGA encapsulated MBs were transferred to a one-necked round bottom flask that contained 10 mL of PVA 1% solution and the suspension was stirred at 100 rpm, 20 °C and 950 mbar for 45 min using a rotary evaporator in order to toughen the synthesized MBs. Next, the obtained MBs were washed three times with water using an external magnetic disk, and then resuspended in water for a final concentration of 10 mg/mL.

TEM, DLS (both size and ζ –potential), IR and magnetic measurement of the room temperature hysteresis loops were used for the characterization of the MBs obtained here and after further functionalization.

2.5. MBs conjugation with neutravidin

MB@PLGA were also functionalized with a layer of PEI for further conjugation with neutravidin (NAV) through glutaraldehyde linking. First, 1.0 mL of MBs with a concentration of 10 mg/mL in water were transferred to a 1.5 mL LoBind Eppendorf® and separated from the supernatant using a MagRack® 6 from Sigma-Aldrich. Then 1.0 mL of 4.0 mg/mL aqueous solution of PEI was added to the MBs and stirred using a Vortex for 1 h. The MB@PEI were washed three times with water by using the magnetic rack MagRack® and, then 1.0 mL of 2.5% glutaraldehyde solution. The mixture was maintained under stirring in the Vortex during 30 min. After that, the reaction was washed three times with water using the MagRack® and, again with the supernatant removed, 1.0 mL of a 0.8 mg/mL solution of NAV in PBS 0.1 M pH 7.2 was added. This suspension was stirred during 6 h using a Vortex and the excess of NAV was removed by washing three-times with PBS 0.1 M pH 7.2 using the MagRack®. Finally, the MB@NAV were suspended in 1 mL of PBS 0.1 M pH 7.2 and maintained under refrigeration until its use.

2.6. Synthesis of AuNPs and conjugation with antibodies

AuNPs were synthesized following the method developed by Turkevich et al. [51]. Briefly, 100 mL of a solution 2.94×10^{-4} M of gold (III) chloride trihydrate were reduced by 2.5 mL of an aqueous solution 3.88×10^{-2} M of tri-sodium citrate dihydrate at boiling point and under vigorous stirring for 15 min. Then, the reaction was moved to a cold magnetic stirrer and maintained under vigorous stirring for 30 min. Past this time, 690 μL of the as-synthesized AuNPs (9.00×10^{14} NPs/mL) were transferred to a 1.5 mL LoBind Eppendorf® tube and centrifuged at 7500 g, 20 °C for 30 min in the presence of 0.025% Tween-20. The supernatant was removed and 700 μL of 2 mM trisodium citrate solution pH 7.3 were added. For the initial direct immunoassay (Section 2.7.), on this solution, 57.5 μL of 100 μg/ mL antibody (human IgG for positive samples and mouse-IgG for negative control) were added and the solution was incubated for 60 min at 25 °C at gentle stirring. Finally, the solution was centrifuged at 7500 g, 4 °C for 20 min and the pellet was resuspended in 0.1 M PBS pH 7.2 with the addition of 1% BSA.

For the sandwich immunoassay for Tau protein detection (Section 2.8.), AuNPs were conjugated with Anti-Tau antibody, following the same procedure with the addition of Anti-Tau antibody in a concentration of 40 μg/mL.

2.7. Direct immunoassay for the evaluation of MB@NAV performance as immunosensing platforms

For the evaluation of the ability of MB@NAV to be used as platforms in an immunoassay, they were conjugated with a biotinylated-anti-human IgG (anti-HIgG). Briefly, 15 μL of a solution 10 mg/mL of MB@NAV were transferred to a 0.5 mL LoBind Eppendorf® tube and washed three-times with B&W buffer using a MagRack®. Then, MB@NAV were re-suspended in 108 μL of B&W buffer, and 42 μL of anti-HIgG (200 μg/mL) were added. The solution was incubated during 30 min at 25 °C and 650 rpm in a Thermo Shaker incubator. After this step, MB@NAV/anti-HIgG were washed three times with B&W buffer and resuspended in 150 μL of BB solution followed by an incubation period of 1 h at 25 °C and 650 rpm to prevent from unspecific absorption by blocking any remaining active sites. MB@NAV/anti-HIgG were then washed three times with B&W buffer and the supernatant removed. Then, 150 μL of AuNPs conjugated with human IgG (HIgG-AuNPs) were added and the solution was incubated for 30 min at 25 °C and 650 rpm. After this step, MB@NAV/anti-HIgG/HIgG were separated and washed two times with B&W buffer and two times with 0.1 M PBS pH 7.2 using a MagRack®. The final product was resuspended in 150 μL of 0.1 M PBS pH 7.2. Negative control assays were performed following the same experimental procedure but using mouse IgG (mIgG-AuNPs) instead of HIgG-AuNPs.

The electrochemical measurements were done taking advantage of the potential of AuNPs as catalysts of hydrogen evolution reaction (HER), following a previously optimized procedure [52,53]. For these measurements, 20 μL of sample were placed on the working area of a SPCEs above a magnetic support and 20 μL of a 0.2 M HCl solution were added. Electrochemical measurements were done by applying an initial potential of + 1.35 V for 60 s and then measuring by chronoamperometry at a fixed potential of −1.00 V for 300 s. The absolute value of the current at 300 s was chosen as the analytical signal.

The same procedure was performed with commercially available streptavidin-modified magnetic beads, for comparison purposes.

2.8. Sandwich immunoassay for Tau protein detection

A similar procedure to the previously described for the direct

immunosensor was done here for the detection of Tau protein. Briefly, 10 μL of the obtained MB@NAV were re-suspended to a final volume of 150 μL with B&W buffer and washed three-times with the same buffer. Then, MB@NAV were re-suspended in 108 μL of B&W buffer and 42 μL of biotinylated anti-Tau antibody (15 μg/mL) were added. The solution was incubated during 30 min at 25 °C and 650 rpm in a Thermo Shaker incubator. After incubation MB@NAV/anti-Tau were washed three-times with B&W buffer, and 150 μL of BB solution were added and incubated for 60 min in the same conditions. Then, another washing step was performed, and 100 μL of Tau protein was added in concentrations ranging from 50 to 750 ng/mL and incubated for 30 min. After the incubation, MB@NAV/anti-Tau/Tau conjugate was washed three-times with B&W buffer and 150 μL of the conjugate of AuNPs with anti-Tau antibody were added for the incubation during 60 min at the same conditions.

The final product was washed twice with B&W buffer and twice with 0.1 M PBS pH 7.2 and measured in SPCEs above a magnetic support with the addition of 20 μL of the final product and 20 μL of 0.2 M HCl, using the same electrochemical procedure as in the direct immunoassay.

2.9. Spike and recovery protocol

Spike and recovery experiment was performed to evaluate if the Tau protein detection was affected by the human serum matrix. A pool of serum samples of healthy patients obtained from the University Program for Seniors of Oviedo University, from the Memory Workshop from the Popular University, from Roces Senior Center, from Gijón-Sur Integrated Cultural Center, from Ateneo Integrated Cultural Center, and from San Agustín Senior Social Center (Spain) were used for such purpose. They met the following criteria: (1) no history of past or current psychiatric or neurological disorders and (2) a score higher than 26 in the Mini-Mental State Examination (MMSE). Also, subjects with acute comorbidities were excluded.

The serum was spiked with different concentrations of Tau (50 and 750 ng/mL) and then evaluated in the immunoassay (n = 3 for each sample), following the same experimental procedure than the described in section 2.8. The analytical signals were compared with those obtained for the standard samples in PBS buffer, calculating the % recovery of the analytical signal in the real matrix sample.

3. Results and discussion

3.1. Synthesis and characterization of ZnFeNPs

ZnFeNPs have been proposed as an alternative to conventional SPIONs since it is known that the introduction of Zn^{2+} ions at the tetrahedral sites of SPIONs may increase the magnetic properties of these particles [54]. For that reason, their use in the formation of superparamagnetic MBs by encapsulation in polymeric matrixes has been postulated as an alternative to traditional SPIONs based MBs in order to improve magnetism without the need to increase the particles size. In this work, ZnFeNPs have been synthesized following a previously published thermal-decomposition method developed by our group but using an appropriate mixture of $Zn(acac)_2$ and $Fe(acac)_3$ instead of using only $Fe(acac)_3$ [50]. This method has advantages over electrochemical-based synthetic routes [55,56] in terms of simplicity, reproducibility and size-controllability [11,57].

Figure 1.A. represents an electron micrograph of ZnFeNPs and the corresponding size distribution. The average size distribution of ZnFeNPs is 13 ± 3 nm with a spherical shape an appropriate polydispersity. ZnFeNPs were also characterized by X-ray powder diffraction (XRDP) (Fig. 1.B.). Compared to the standard Fe_3O_4, ZnFeNPs have a similar profile. To estimate the crystallinity domain size of the nanoparticles, a LeBail fitting method was performed using magnetite as standard sample, showing an average apparent size of 15 ± 9 nm, a value that is within the range of that observed by TEM, also indicating that the ZnFeNPs are monocrystalline.

Composition of ZnFeNPs was also studied by ICP-MS, that provided a Zn/Fe ratio of 12:88 (±1), what indicates that the obtained NPs are dopped with Zn. Additionally, it was proven that little modifications in the Zn/Fe ratio do not affect significantly their magnetic behavior (Table S1.). ZnFeNPs were also characterized by IR (Fig. 1.C.), showing a broad band at 570 cm^{-1}, due to solid-state vibrations of ferrites. The obtained ZnFeNPs were covered by oleic acid, what is confirmed by the

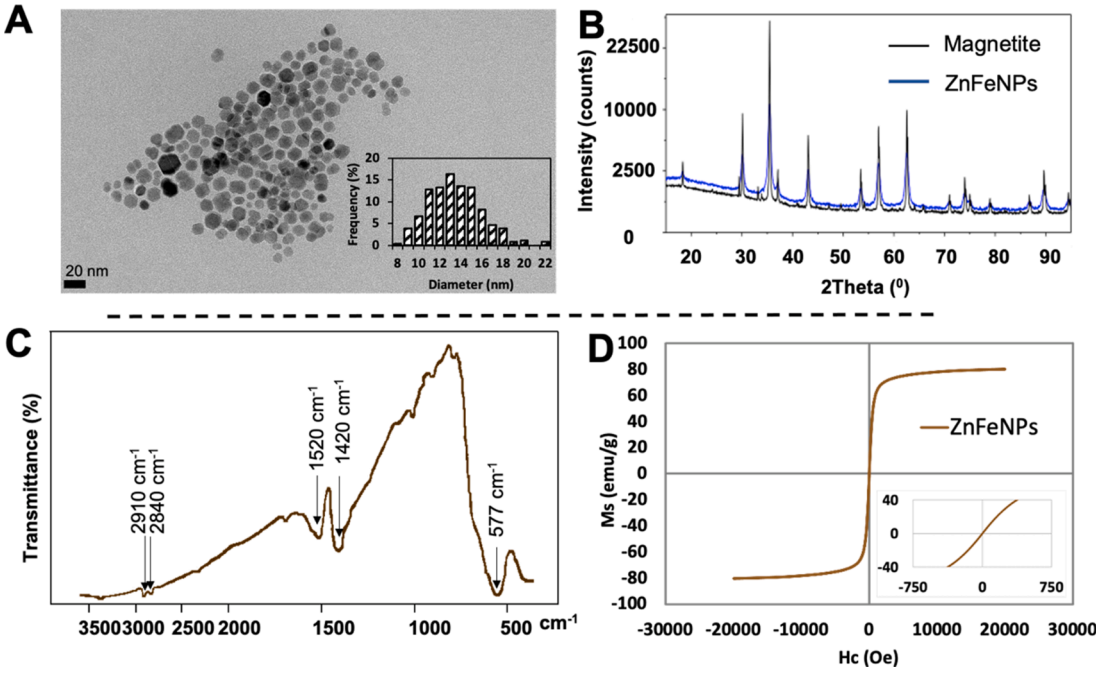

Fig. 1. Characterization of ZnFeNPs. **A.** Electron micrographs of ZnFeNPs and size distribution histogram showing an average size diameter of 13 nm; **B.** XRDP analysis of ZnFeNPs compared to magnetite as reference material. ZnFeNPs pattern presents a broadened profile; **C.** IR spectrum of ZnFeNPs; and **D.** Hysteresis curve of ZnFeNPs that shows a superparamagnetic behavior and a Ms of 81 emu/g (inset shows amplified the low-field region of the hysteresis curve).

presence of absorption bands of the oleate at ~ 2910 cm^{-1}, w, and ~ 2840 cm^{-1}, w (CH stretching), and ~ 1520 cm^{-1}, w, br and ~ 1420 cm^{-1}, w, br (symmetric and antisymmetric stretching of –COO). This IR spectra is equal to the previously described for magnetite NPs [50] what suggests that the incorporation of Zn ions is by doping of the magnetite nanoparticles, as expected.

The magnetic hysteresis curve of ZnFeNPs (Fig. 1.D.) showed a superparamagnetic behavior at room temperature, with a coercivity of 3 Oe and a saturation magnetization (Ms) of 81 ± 1 emu/g, which is much higher than the previously described for magnetite NPs obtained by the same synthetic method (12 Oe and 70 emu/g) [50]. Similar increases in the value of Ms have been described for other zinc doped magnetite [14–16,54].

3.2. Synthesis and characterization of magnetic beads (MBs)

The obtained ZnFeNPs were used for the formation of MBs following the procedure described in Fig. 2, based on previously published methods with some modifications [58–60]. A dispersion of ZnFeNPs in 2-propanol was mixed with PLGA in DMF solution and incorporated into an aqueous phase of PVA, following a water in oil emulsion method. The contact of these two phases facilitates the assembling of ZnFeNPs and PLGA, leading to the formation of the MBs. PLGA is a biocompatible polymer widely used in drug delivery due to its effective encapsulation capacity and control release [61], what provides a great versatility to the MBs obtained in this work [62,63]. MB@PLGA were also coated with a layer of PEI (MB@PEI) in order to achieve an improved encapsulation and stability. Also, PEI was selected as it facilitates the conjugation due to i) the primary amine groups of PEI and to ii) the well-known proton sponge effect of this polymer, associated to its high positive charge that facilitates the electrostatic interaction with negatively charged biomolecules [64,65].

In order to obtain MBs suitable for their use as immunosensing platforms, the synthesized MB@PEI need to be functionalized with affinity proteins. To facilitate the comparison of the MBs synthesized in this work with commercially available ones, neutravidin (NAV) affinity protein was selected for the conjugation. NAV is, together with streptavidin, a biotin-recognition protein normally used as molecular recognition element in biosensing [66]. In this work, NAV was incorporated through glutaraldehyde as a crosslinker, thanks to its high reactivity [67]. This methodology may also be applied to different affinity proteins, thus increasing the versatility of the obtained MBs.

The obtained MBs were characterized in terms of size, DLS, ζ -potential, IR and magnetic behavior by measuring the hysteresis loops at room temperature.

First, MBs were morphologically characterized, showing a spherical

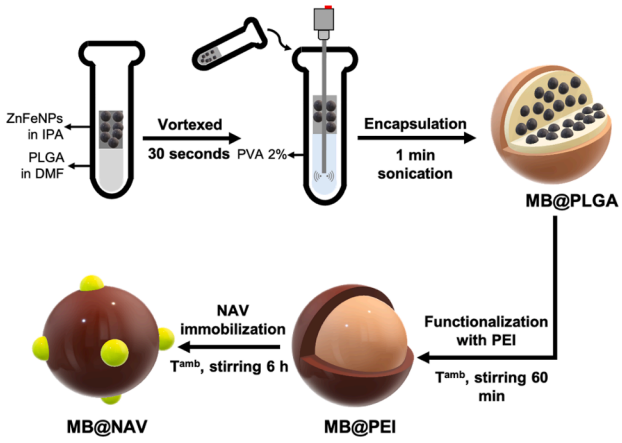

Fig. 2. Schematic representation of the encapsulation-based assembly method for the synthesis of MB@NAV.

shape and an enhanced dispersity with an average diameter of 89 ± 18 nm for MB@PLGA, 96 ± 16 nm for MB@PEI and 117 ± 19 nm for MB@NAV (Fig. 3.A.) obtained from the TEM images. It is worthy mention that the encapsulation observed in the MB@PLGA is slightly worse as noticed in the left side inset in Fig. 3.A., while this state is corrected after the incorporation of PEI. The presence of external NAV is correlated with the increased size of the final NP, as detected by DLS.

As it can be clearly seen, each MB is constituted by a large number of individual ZnFeNPs. Considering the average volume of a MB and the average volume of a single ZnFeNP, it has been estimated that each MB is constituted by approximately 260 individuals ZnFeNPs (assuming that there are no holes inside the particle).

Measurement of the hydrodynamic size of the as-synthesized MBs indicates a change in the diameter of the particles after functionalization, going from 182 nm of MB@PLGA (Polydispersity index (PdI) of 0.098), 216 nm for MB@PEI (PdI of 0.147) to 414 nm (PdI 0.318) after the incorporation of NAV (Fig. 3.B.), what tallies with the presence of this high molecular weight protein (~60 kDa). It is also worthy to mention that an increase in the PdI of the particles is also noticed, what suggests that the conjugation with NAV slightly favor aggregation compared to previous steps.

Functionalization has also been confirmed by measuring the ζ -potential of MBs, which represents the external electrical potential in the surface of the suspended particles [68]. The ζ -potential (Fig. 3.C.) of MB@PLGA suspended in milli-Q water was of −10 ± 5 mV due to the presence of external carboxylic groups own of acid terminations of the PLGA used. After the coating with PEI, the ζ -potential changed to a positive value of 27 ± 6 mV, corresponding to the presence of amine groups, confirming the successful incorporation of PEI. ζ -potential of MB@NAV measured in PBS 0.1 M pH 7.2 shifts from 27 ± 6 mV to −10 ± 5 mV, what correlates with the charge of NAV near its isoelectric point (pH 6.3) [69].

In order to furtherly confirm the functionalization, MBs were characterized by IR (Fig. 3.D.). The presence of the poly(lactic-co-glycolic) matrix in MB@PLGA nanoparticles is denoted mainly by the band at 1752 cm^{-1}, due to the ester carbonyl group ($\nu_{C=O}$) of the copolymer. It should be noticed the relative intensities of the peaks at 1422 and 1384 cm^{-1} in the same IR spectrum, assignable to the C–H bending vibrations of the CH_3 and CH_2 groups. The stronger intensity of the band at 1384 cm^{-1} indicates the presence of abundant methyl groups, as it is expected for the lactic repeating unit in PLGA [70]. Other absorptions of interest are those at 1167 and 1090 cm^{-1}, due to the C-O-C groups of the polyester.

On the other hand, the most characteristic band of the PEI assigned to N–H bending should appear at 1576 cm^{-1} [71]. However, in the infrared spectrum of the MB@PEI this peak is almost completely hidden by a δ_{OH} band at 1636 cm^{-1}, probably due to the presence of water. It should be mentioned that the intensities of the peaks at 1422 and 1384 cm^{-1} are very similar, as expected, considering the predominant presence of CH_2 groups in PEI. Additionally, bands corresponding to PLGA still remain, confirming that the incorporation of PEI does not remove the previously present PLGA.

Moreover, the presence of NAV could not be clearly identified through IR due to the multiple functional groups that compose this protein and to the previous structure of the MBs, although it could be seen an increase in the signal corresponding to ~ 1545 cm^{-1}. This peak corresponds to amide II band of the secondary amides present in the NAV protein.

Magnetic behavior of all the obtained MBs was measured at room temperature (Fig. 3.E.). The saturation magnetization (Ms) of MB@PLGA was of 54 ± 2 emu/g, while after the coating with PEI this value increased to 63 ± 5 emu/g. Although it should be expected a decrease in Ms with the increase of non-magnetic components [72], the higher degree of encapsulation observed through TEM measurements for MB@PEI and the purification stages performed after functionalization has allowed us to separate and purify those MBs with an increased

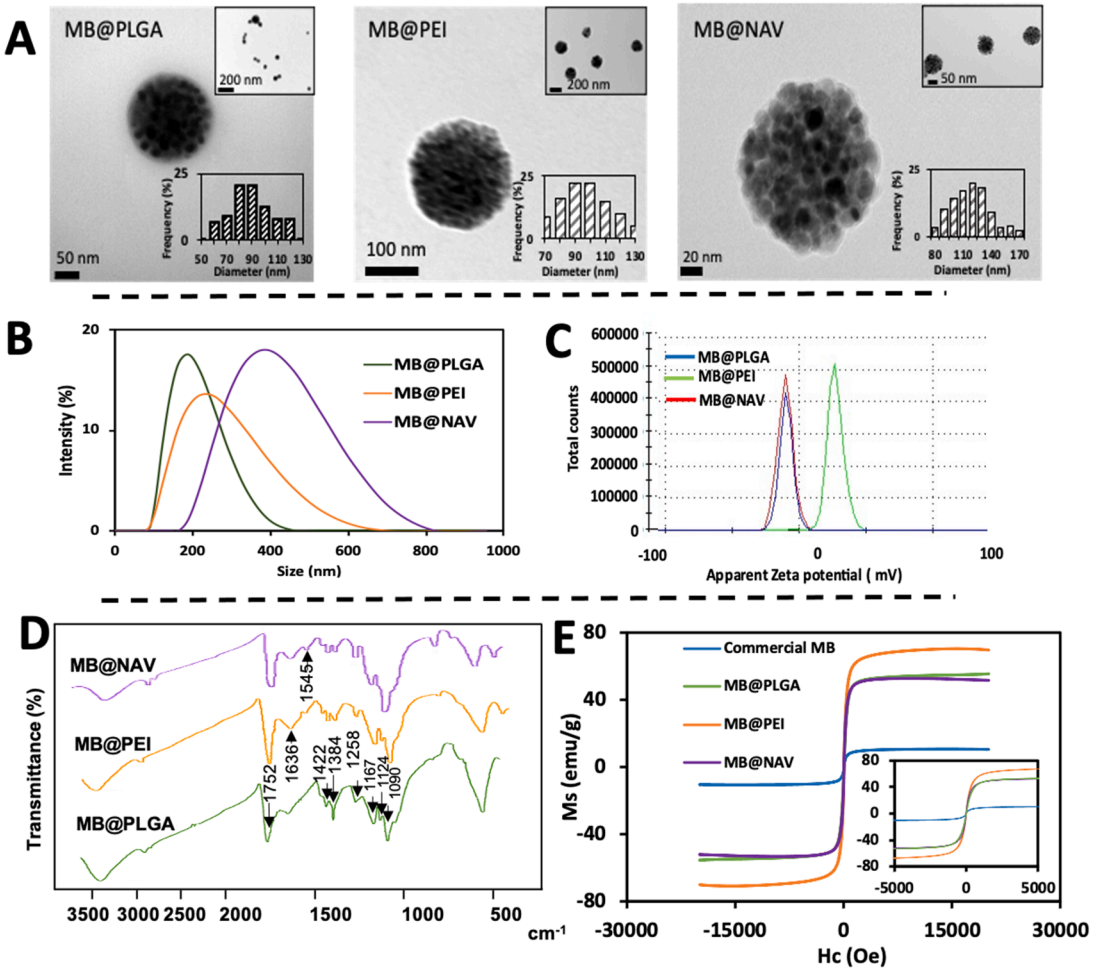

Fig. 3. Characterization of MBs. **A.** TEM micrographs of MB@PLGA, MB@PEI and MB@NAV and the corresponding size distribution histogram. An inset of higher magnification is included in the right side of the micrographs; **B.** Hydrodynamic diameter of all MBs in which it is observed a change after functionalization; **C.** ζ -potential showing a shift from a negative value for MB@PLGA (external carboxylic groups) to a positive value for MB@PEI (external amine groups) and again, to a negative value after the incorporation of NAV (external imine groups); **D.** IR spectrum of MB@PLGA, MB@PEI and MB@NAV; and **E.** Hysteresis curves of MB@PLGA (54 emu/g), MB@PEI (63 emu/g), MB@NAV (54 emu/g) and the commercially available MBs (11 emu/g). Inset represents an amplification of the low-field region of the hysteresis curves.

magnetic saturation, what could explain the improvement observed.

Regarding superparamagnetic behavior, MB@PLGA present a reduced remanence with a coercivity of 10 Oe, what indicates that the clustering of individual ZnFeNPs into MBs allows to maintain the superparamagnetic behavior of the individual nanoparticles. This value increases to 14 Oe after the incorporation of PEI. Regarding the magnetic behavior of MB@NAV, it is observed a slight decrease in the Ms (from 63 ± 5 emu/g to 54 ± 1 emu/g) and an increase in the coercivity (from 14 to 16 Oe) of the particles. Commercially available MB were also measured for comparison purposes, showing a Ms of 11 emu/g with a coercivity of 2 Oe. The low value of total *m* noticed for such MBs is probably due to the high proportion of non-magnetic material, as previously reported [21].

3.3. Direct immunoassay for the evaluation of MB@NAV performance

A direct immunoassay was performed for i) the evaluation of the ability of the MB@NAV to be used as immunosensing platforms and ii) as a comparison of the performance of the MB@NAV with that of the commercial MBs. Both MB@NAV and commercial MBs were bioconjugated with biotinylated anti-human IgG (anti-HIgG) and let to react with human IgG (HIgG), previously conjugated with AuNP tags. Mouse IgG (MIgG) conjugated with AuNPs was used as negative control (Fig. 4.A.). Electrochemical detection was based on the electrocatalytic activity of AuNPs toward the hydrogen evolution reaction (HER) [73], by applying a potential of −1.0 V during 300 s, selecting the value of the current recorded at 300 s as the analytical signal [52,74].

Figure 4.B. shows the chronoamperograms recorded during the stage of hydrogen ion electroreduction for the different assays evaluated. An increase in the catalytic current is clearly observed for the positive assays compared with the control ones. The comparison of the average analytical signals and their standard deviation (n = 3) shown in Fig. 4.C. suggest that MB@NAV have a better performance than the commercial ones. First, positive samples provide higher signals, which suggests an enhanced ability of the MB@NAV to capture antibodies. Moreover, the signals recorded for negative control samples were smaller for the MB@NAV, what may indicate a lower unspecific absorption of protein/AuNP conjugates. In addition, the reproducibility obtained with MB@NAV was better than that of the commercial MBs, giving a relative standard deviation (RSD) of 4% (RSD of 12% for commercial MBs).

3.4. Sandwich immunoassay for the detection of Tau protein using MB@NAV

Once evaluated the ability of the MB@NAV to efficiently act as immunosensing platform, they were applied for the detection of Tau

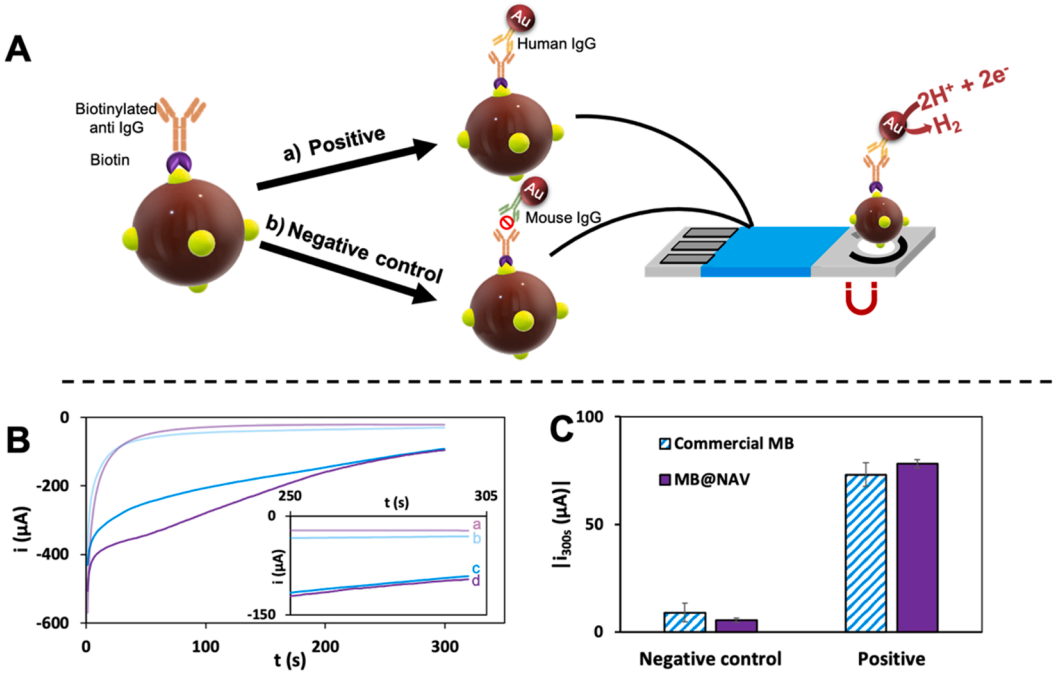

Fig. 4. Direct immunoassay for the evaluation of MB@NAV performance. **A.** Schematic representation of the direct immunoassay performed for the evaluation of the MB@NAV performance; **B.** Chronoamperograms recorded by applying a potential of −1.00 V for 300 s in 1 M HCl for: a. Negative control with MB@NAV, b. negative control with commercial MBs, c. positive control with commercial MBs and d. positive control with MB@NAV (inset shows an amplification of the region near 300 s); **C.** Current obtained at 300 s (analytical signal) for the negative control and positive control with both MB@NAV synthesized in this work (purple) and commercial MBs (blue lines). Background current of 16.5 μA corresponding to the hydrogen evolution in the bare carbon electrode was subtracted from all measurements.

protein, an AD biomarker, in a sandwich immunoassay format. The structure of the immunoassay is schematized in Fig. 5.A. Briefly, a biotinylated anti-Tau antibody was immobilized on the MB@NAV and the conjugate was then incubated with samples containing concentrations of Tau protein ranging from 50 to 750 ng/mL, in a dose–response assay. The sandwich was then completed with anti-Tau antibody conjugated with AuNPs, that were detected based on the HER reaction, as described above.

The results obtained are represented in Fig. 5.B. and depict that there is a direct correlation between the catalytic current recorded and the concentration of Tau protein. Fig. 5.C. shows that there is a good linear relationship between the two parameters in the range 50–750 ng/mL, with a correlation coefficient of 0.9963, according to the equation:

$$Current_{300s} = 0.1264[Tau](ng/mL) + 63.043$$

The limit of detection (LOD) was calculated as three times the standard deviation of the intercepted divided by the slope, resulting in a value of 63 ng/mL. The method showed an excellent reproducibility, with an average relative standard deviation (RSD) of 4 % (n = 3).

Tau protein has been selected as model analyte in our proof-of-

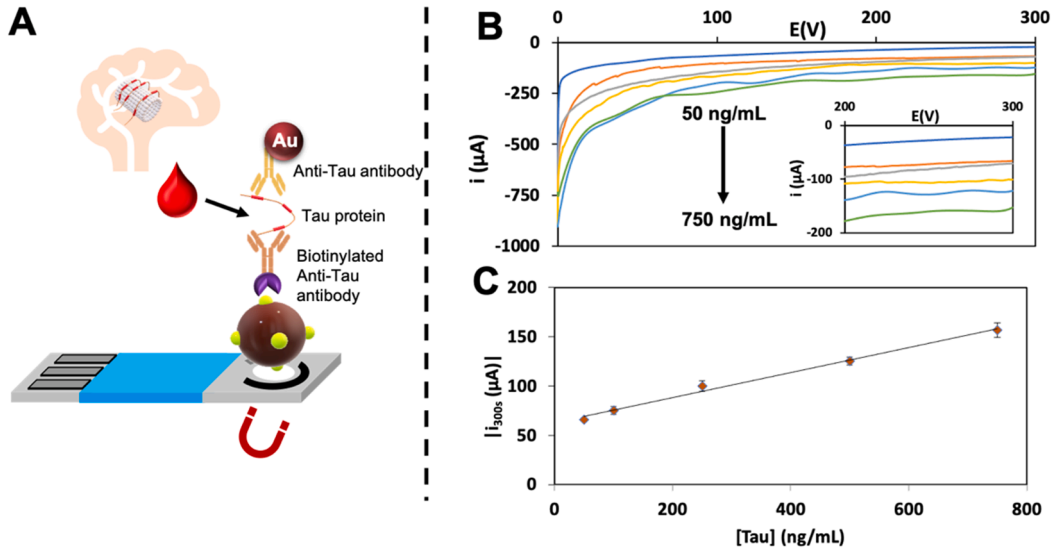

Fig. 5. **A**. Schematic representation of the biosensor used for the detection of Tau protein by the immobilization of biotinylated anti-Tau antibodies onto MB@NAV; **B.** Chronoamperograms recorded by applying a potential of −1.00 V for 300 s in 0.1 M HCl for each Tau concentration ranging between 50 and 750 ng/mL. Inside, an inset of the signal recorded at the region near 300 s; **C.** Calibration curve of the current recorded at 300 s for each Tau concentration.

concept, instead of i.e. hyperphosphorylated one due to the following reasons. Although there is still controversy on the clinical implications of total Tau protein as predictor of neurodegeneration [75,76] and its role in AD, there is no consensus on hyperphosphorylated Tau (p-tau) too, as it is not clear which p-tau isoform is more relevant in AD. Even though p-tau181 has been mainly stated as AD biomarker in blood [77], the role of p-tau217 has also stood out [78,79]. The difference between both isoforms relies on the amino acid residue that is phosphorylated. These clinical results point out that the mechanism of action of Tau protein in AD still requires further investigation. For these reasons, the identification of Tau protein as proof-of-concept is an extended practice in immunosensing for AD diagnostics [36].

This is way we have selected Tau protein as analyte in our proof-of-concept work. It is worthy to highlight that our biosensing system may be easily adapted to the determination of p-tau, just using suitable antibodies that are commercially available.

3.5. Tau protein analysis in human serum samples: Spike and recovery

The final objective of the development of an analytic biosensor is the detection of biomolecules in real samples. In this context, it has been evaluated the performance of the biosensor in a serum sample of cognitively healthy patients, demonstrating the selectivity of the analytical method in the real scenario. For that purpose, a spike and recovery method was performed obtaining a high recovery rate at levels around 85–89% (Table 1). These results indicate that the presence of other components in real samples do not significantly interfere in the accurate detection of Tau protein, opening the way to the use of the here described methodology to the evaluation of samples from AD patients.

4. Conclusions

In this work, we report a novel method for obtaining magnetic beads (MBs) with improved performance as immunosensing platforms, which is applied for the detection of Tau protein, an Alzheimer's disease biomarker in human serum.

First, ZnFeNPs were obtained by a thermal-decomposition method, demonstrating that the doping with Zn atoms of the magnetite nanoparticles, clearly enhances their magnetic behavior. The obtained ZnFeNPs are used for the formation of MBs by encapsulation in a PLGA polymeric matrix. In order to facilitate their use as immunosensing platform, MB@PLGA were first functionalized with PEI and then NAV was furtherly immobilized on their surface. In all cases, MBs maintained their superparamagnetic behavior with high saturation magnetization values, assuring that encapsulation of single nanoparticles works as a way of maintaining magnetism while allowing further functionalization. Moreover, the saturation magnetization obtained for the as-synthesized MB@NAV was significantly higher than that of commercial MBs, constituting an important practical advantage.

The performance of MB@NAV in a direct immunoassay for detecting HIgG using AuNPs as labels showed lower RSD for MB@NAV compared to commercial MBs, thus improving the reproducibility of the assay. Moreover, the lower and higher net currents recorded with MB@NAV for control and positive samples respectively suggested that the here described MBs provide lower non-specific adsorptions as they have a greater surface functionalization ability.

These results prove the effectivity of the obtained MB@NAV as immunosensing platforms, and their versatility opens the way to their use for a wide variety of applications.

The developed immunosensor for Tau protein detection constitutes just a proof-of-concept of the potential ability of such MBs to be used as immunosensing platforms for an interesting application in real samples. The low matrix effects (high recoveries) observed in human serum samples demonstrate the excellent performance of our MBs in a real scenario. Although the detection limit obtained in our proof-of-concept study (63 ng/mL) is higher than the required for AD diagnostics (pg/mL levels in human serum), the versatility of both the MBs and the nanoparticle tags allow to make feasible further optimizations for meeting such clinical needs. On the one hand, it is well-known that the magnetic separation performed after each incubation step allows to preconcentrate the sample. This means that higher sample volumes than the evaluated in our work (100 μL) may be assayed, capturing a higher amount of the AD biomarker. After removing the supernatant, MBs may be re-suspended in a smaller volume, leading to the sample preconcentration. Regarding the tag, current research in our group (and others) is focused on alternative bimetallic nanoparticles with electrocatalytic properties that can be detected at lower levels than the AuNPs.

Such studies, together with a careful evaluation of patient samples will be object of future research.

Table 1
Spike and recovery assay data.

Sample	Spiked Tau (ng/mL)	Current in PBS (μA)	Current in real sample (μA)	Recovery (%)
Serum from cognitively healthy subjects	50	−66,12	−56,15	85%
	750	−156,8	−139,0	89%

Declaration of Competing Interest

The authors declare that they have no known competing financial interests or personal relationships that could have appeared to influence the work reported in this paper.

Acknowledgements

This work has been supported by the CTQ2017-86994-R and MCI-21-PID2020-115204RB-I00 projects from the Spanish Ministry of Economy and Competitiveness (MINECO) and the Spanish Ministry of Science and Innovation (MICINN) respectively and the FC-GRUPIN-ID/2018/000166 project from the Asturias Regional Government. C. Toyos-Rodríguez thanks the MICINN for the award of a FPI Grant (PRE2018-084953). A. de la Escosura-Muñiz also acknowledges the MICINN for the "Ramón y Cajal" Research Fellow (RyC-2016-20299).

Appendix A. Supplementary data

Supplementary data to this article can be found online at https://doi.org/10.1016/j.microc.2022.107211.

References

[1] S. Mirza, M.S. Ahmad, M.I.A. Shah, M. Ateeq, in: Metal Nanoparticles for Drug Delivery and Diagnostic Applications, Elsevier, 2020, pp. 189–213, https://doi.org/10.1016/B978-0-12-816960-5.00011-2.
[2] L.H. Reddy, J.L. Arias, J. Nicolas, P. Couvreur, Magnetic nanoparticles: design and characterization, toxicity and biocompatibility, pharmaceutical and biomedical applications, Chem. Rev. 112 (11) (2012) 5818–5878, https://doi.org/10.1021/cr300068p.
[3] S.C.N. Tang, I.M.C. Lo, Magnetic nanoparticles: essential factors for sustainable environmental applications, Water Res. 47 (8) (2013) 2613–2632, https://doi.org/10.1016/j.watres.2013.02.039.
[4] Y. Xu, E. Wang, Electrochemical biosensors based on magnetic micro/nano particles, Electrochim. Acta 84 (2012) 62–73, https://doi.org/10.1016/j.electacta.2012.03.147.
[5] M. Ahmadi, A. Ghoorchian, K. Dashtian, M. Kamalabadi, T. Madrakian, A. Afkhami, Application of magnetic nanomaterials in electroanalytical methods: A review, Talanta 225 (2021) 121974, https://doi.org/10.1016/j.talanta.2020.121974.
[6] A.-H. Lu, E.L. Salabas, F. Schüth, Magnetic Nanoparticles: Synthesis, Protection, Functionalization, and Application, Angew. Chem. Int. Ed. 46 (8) (2007) 1222–1244, https://doi.org/10.1002/anie.200602866.
[7] R.B. Nasir Baig, M.N. Nadagouda, R.S. Varma, Magnetically retrievable catalysts for asymmetric synthesis, Coord. Chem. Rev. 287 (2015) 137–156, https://doi.org/10.1016/j.ccr.2014.12.017.

[8] Y.-T. Chen, A.G. Kolhatkar, O. Zenasni, S. Xu, T.R. Lee, Biosensing Using Magnetic Particle Detection Techniques, Sensors. 17 (2017) 2300, https://doi.org/10.3390/s17102300.

[9] L. Li, Y. Yang, J. Ding, J. Xue, Synthesis of Magnetite Nanooctahedra and Their Magnetic Field-Induced Two-/Three-Dimensional Superstructure, Chem. Mater. 22 (10) (2010) 3183–3191.

[10] Q. Li, C.W. Kartikowati, S. Horie, T. Ogi, T. Iwaki, K. Okuyama, Correlation between particle size/domain structure and magnetic properties of highly crystalline Fe3O4 nanoparticles, Sci Rep. 7 (2017) 9894, https://doi.org/10.1038/s41598-017-09897-5.

[11] D. Ling, T. Hyeon, Chemical Design of Biocompatible Iron Oxide Nanoparticles for Medical Applications, Small. 9 (9-10) (2013) 1450–1466, https://doi.org/10.1002/smll.201202111.

[12] C.G.C.M. Netto, H.E. Toma, L.H. Andrade, Superparamagnetic nanoparticles as versatile carriers and supporting materials for enzymes, J. Mol. Catal. B Enzym. 85–86 (2013) 71–92, https://doi.org/10.1016/j.molcatb.2012.08.010.

[13] K. Aguilar-Arteaga, J.A. Rodriguez, E. Barrado, Magnetic solids in analytical chemistry: A review, Anal. Chim. Acta 674 (2) (2010) 157–165, https://doi.org/10.1016/j.aca.2010.06.043.

[14] J.-T. Jang, H. Nah, J.-H. Lee, S. Moon, M. Kim, J. Cheon, Critical Enhancements of MRI Contrast and Hyperthermic Effects by Dopant-Controlled Magnetic Nanoparticles, Angew. Chem. Int. Ed. 48 (7) (2009) 1234–1238, https://doi.org/10.1002/anie.200805149.

[15] J.M. Byrne, V.S. Coker, E. Cespedes, P.L. Wincott, D.J. Vaughan, R.A.D. Pattrick, G. van der Laan, E. Arenholz, F. Tuna, M. Bencsik, J.R. Lloyd, N.D. Telling, Biosynthesis of Zinc Substituted Magnetite Nanoparticles with Enhanced Magnetic Properties, Adv. Funct. Mater. 24 (17) (2014) 2518–2529, https://doi.org/10.1002/adfm.201303230.

[16] I. Castellanos-Rubio, O. Arriortua, L. Marcano, I. Rodrigo, D. Iglesias-Rojas, A. Barón, A. Olazagoitia-Garmendia, L. Olivi, F. Plazaola, M.L. Fdez-Gubieda, A. Castellanos-Rubio, J.S. Garitaonandia, I. Orue, M. Insausti, Shaping Up Zn-Doped Magnetite Nanoparticles from Mono- and Bimetallic Oleates: The Impact of Zn Content, Fe Vacancies, and Morphology on Magnetic Hyperthermia Performance, Chem. Mater. 33 (9) (2021) 3139–3154, https://doi.org/10.1021/acs.chemmater.0c0479410.1021/acs.chemmater.0c04794.s001.

[17] O. Philippova, A. Barabanova, V. Molchanov, A. Khokhlov, Magnetic polymer beads: Recent trends and developments in synthetic design and applications, Eur. Polym. J. 47 (4) (2011) 542–559, https://doi.org/10.1016/j.eurpolymj.2010.11.006.

[18] Z. Lu, Y. Yin, Colloidal nanoparticle clusters: functional materials by design, Chem. Soc. Rev. 41 (21) (2012) 6874, https://doi.org/10.1039/c2cs35197h.

[19] J. Guo, W. Yang, C. Wang, Magnetic Colloidal Supraparticles: Design, Fabrication and Biomedical Applications, Adv. Mater. 25 (37) (2013) 5196–5214, https://doi.org/10.1002/adma.201301896.

[20] N.C. Bigall, C. Wilhelm, M.-L. Beoutis, M. García-Hernandez, A.A. Khan, C. Giannini, A. Sánchez-Ferrer, R. Mezzenga, M.E. Materia, M.A. Garcia, F. Gazeau, A.M. Bittner, L. Manna, T. Pellegrino, Colloidal Ordered Assemblies in a Polymer Shell—A Novel Type of Magnetic Nanobeads for Theranostic Applications, Chem. Mater. 25 (7) (2013) 1055–1062, https://doi.org/10.1021/cm3036746.

[21] J. Park, M.D. Porter, M.C. Granger, Colloidally Assembled Zinc Ferrite Magnetic Beads: Superparamagnetic Labels with High Magnetic Moments for MR Sensors, ACS Appl. Mater. Interfaces. 9 (23) (2017) 19569–19577, https://doi.org/10.1021/acsami.7b0318210.1021/acsami.7b03182.s001.

[22] S.H. Chun, S.W. Shin, L. Amornkitbamrung, S.Y. Ahn, J.S. Yuk, S.J. Sim, D. Luo, S. H. Um, Polymeric Nanocomplex Encapsulating Iron Oxide Nanoparticles in Constant Size for Controllable Magnetic Field Reactivity, Langmuir 34 (43) (2018) 12827–12833, https://doi.org/10.1021/acs.langmuir.7b0414310.1021/acs.langmuir.7b04143.s001.

[23] S.-J. Lee, H.-J. Kim, Y.-M. Huh, I.W. Kim, J.H. Jeong, J.-C. Kim, J.-D. Kim, Functionalized Magnetic PLGA Nanospheres for Targeting and Bioimaging of Breast Cancer, J Nanosci Nanotechnol. 18 (3) (2018) 1542–1547, https://doi.org/10.1166/jnn.2018.14220.

[24] N. Schleich, P. Sibret, P. Danhier, B. Ucakar, S. Laurent, R.N. Muller, C. Jérôme, B. Gallez, V. Préat, F. Danhier, Dual anticancer drug/superparamagnetic iron oxide-loaded PLGA-based nanoparticles for cancer therapy and magnetic resonance imaging, Int. J. Pharm. 447 (1-2) (2013) 94–101, https://doi.org/10.1016/j.ijpharm.2013.02.042.

[25] S.-J. Lee, J.-R. Jeong, S.-C. Shin, J.-C. Kim, Y.-H. Chang, K.-H. Lee, J.-D. Kim, Magnetic enhancement of iron oxide nanoparticles encapsulated with poly(d, l-latide-co-glycolide), Colloids Surf., A 255 (1-3) (2005) 19–25, https://doi.org/10.1016/j.colsurfa.2004.12.019.

[26] A. Jonderian, R. Maalouf, Formulation and In vitro Interaction of Rhodamine-B Loaded PLGA Nanoparticles with Cardiac Myocytes, Front. Pharmacol. 7 (2016), https://doi.org/10.3389/fphar.2016.00458.

[27] L. Gomes dos Reis, W.-H. Lee, M. Svolos, L.M. Moir, R. Jaber, N. Windhab, P. M. Young, D. Traini, Nanotoxicologic Effects of PLGA Nanoparticles Formulated with a Cell-Penetrating Peptide: Searching for a Safe pDNA Delivery System for the Lungs, Pharmaceutics. 11 (2019) 12, https://doi.org/10.3390/pharmaceutics11010012.

[28] T.A.P. Rocha-Santos, Sensors and biosensors based on magnetic nanoparticles, TrAC. 62 (2014) 28–36, https://doi.org/10.1016/j.trac.2014.06.016.

[29] J. Pansieri, M. Gerstenmayer, F. Lux, S. Mériaux, O. Tillement, V. Forge, B. Larrat, C. Marquette, Magnetic Nanoparticles Applications for Amyloidosis Study and Detection: A Review, Nanomaterials. 8 (2018) 740, https://doi.org/10.3390/nano8090740.

[30] M. Pedrero, S. Campuzano, J.M. Pingarrón, Magnetic Beads-Based Electrochemical Sensors Applied to the Detection and Quantification of Bioterrorism/Biohazard Agents, Electroanalysis 24 (2012) 470–482, https://doi.org/10.1002/elan.201100528.

[31] L. Fabiani, M. Saroglia, G. Galatà, R. De Santis, S. Fillo, V. Luca, G. Faggioni, N. D'Amore, E. Regalbuto, P. Salvatori, G. Terova, D. Moscone, F. Lista, F. Arduini, Magnetic beads combined with carbon black-based screen-printed electrodes for COVID-19: A reliable and miniaturized electrochemical immunosensor for SARS-CoV-2 detection in saliva, Biosens. Bioelectron. 171 (2021) 112686, https://doi.org/10.1016/j.bios.2020.112686.

[32] K.e. Luo, K.-B. Jeong, S.-M. You, D.-H. Lee, Y.-R. Kim, Molecular Rearrangement of Glucans from Natural Starch To Form Size-Controlled Functional Magnetic Polymer Beads, J. Agric. Food Chem. 66 (26) (2018) 6806–6813, https://doi.org/10.1021/acs.jafc.8b0159010.1021/acs.jafc.8b01590.s001.

[33] K. Luo, D.-H. Lee, H.J. Adra, Y.-R. Kim, Synthesis of monodisperse starch microparticles through molecular rearrangement of short-chain glucans from natural waxy maize starch, Carbohydr. Polym. 218 (2019) 261–268, https://doi.org/10.1016/j.carbpol.2019.05.001.

[34] A. Iglesias-Mayor, O. Amor-Gutiérrez, A. Novelli, M.-T. Fernández-Sánchez, A. Costa-García, A. de la Escosura-Muñiz, Bifunctional Au@Pt/Au core@shell Nanoparticles As Novel Electrocatalytic Tags in Immunosensing: Application for Alzheimer's Disease Biomarker Detection, Anal. Chem. 92 (10) (2020) 7209–7217, https://doi.org/10.1021/acs.analchem.0c00760.

[35] L. Rivas, A. de la Escosura-Muñiz, J. Pons, A. Merkoçi, Alzheimer Disease Biomarker Detection Through Electrocatalytic Water Oxidation Induced by Iridium Oxide Nanoparticles, Electroanalysis 26 (2014) 1287–1294, https://doi.org/10.1002/elan.201400027.

[36] C.A. Razzino, V. Serafín, M. Gamella, M. Pedrero, A. Montero-Calle, R. Barderas, M. Calero, A.O. Lobo, P. Yáñez-Sedeño, S. Campuzano, J.M. Pingarrón, An electrochemical immunosensor using gold nanoparticles-PAMAM-nanostructured screen-printed carbon electrodes for tau protein determination in plasma and brain tissues from Alzheimer patients, Biosens. Bioelectron. 163 (2020) 112238, https://doi.org/10.1016/j.bios.2020.112238.

[37] C. Toyos-Rodríguez, F.J. García-Alonso, A. de la Escosura-Muñiz, Electrochemical Biosensors Based on Nanomaterials for Early Detection of Alzheimer's Disease, Sensors. 20 (2020) 4748, https://doi.org/10.3390/s20174748.

[38] A. de la Escosura-Muñiz, Z. Plichta, D. Horák, A. Merkoçi, Alzheimer′s disease biomarkers detection in human samples by efficient capturing through porous magnetic microspheres and labelling with electrocatalytic gold nanoparticles, Biosens. Bioelectron. 67 (2015) 162–169, https://doi.org/10.1016/j.bios.2014.07.086.

[39] P. Scheltens, K. Blennow, M.M.B. Breteler, B. de Strooper, G.B. Frisoni, S. Salloway, W.M. Van der Flier, Alzheimer's disease, The Lancet. 388 (10043) (2016) 505–517, https://doi.org/10.1016/S0140-6736(15)01124-1.

[40] A. Kaushik, R.D. Jayant, S. Tiwari, A. Vashist, M. Nair, Nano-biosensors to detect beta-amyloid for Alzheimer's disease management, Biosens. Bioelectron. 80 (2016) 273–287, https://doi.org/10.1016/j.bios.2016.01.065.

[41] B. Shui, D. Tao, A. Florea, J. Cheng, Q. Zhao, Y. Gu, W. Li, N. Jaffrezic-Renault, Y. Mei, Z. Guo, Biosensors for Alzheimer's disease biomarker detection: A review, Biochimie 147 (2018) 13–24, https://doi.org/10.1016/j.biochi.2017.12.015.

[42] K. Iqbal, F. Liu, C.-X. Gong, I. Grundke-Iqbal, Tau in Alzheimer Disease and Related Tauopathies, CAR. 7 (2010) 656–664, https://doi.org/10.2174/156720510793611592.

[43] K. Iqbal, A. del C. Alonso, C.-X. Gong, S. Khatoon, J.-J. Pei, J.Z. Wang, I. Grundke-Iqbal, Mechanisms of neurofibrillary degeneration and the formation of neurofibrillary tangles, in: K. Jellinger, F. Fazekas, M. Windisch (Eds.), Ageing and Dementia, Springer Vienna, Vienna, 1998: pp. 169–180. https://doi.org/10.1007/978-3-7091-6467-9_15.

[44] K. Iqbal, T. Zaidi, G. Wen, I. Grundke-Iqbal, P. Merz, S. Shaikh, H. Wisniewski, I. Alafuzoff, B. Winblad, Defective brain microtubule assembly in Alzheimer's disease, The Lancet. 328 (8504) (1986) 421–426.

[45] Y. Zhou, J. Shi, D. Chu, W. Hu, Z. Guan, C.-X. Gong, K. Iqbal, F. Liu, Relevance of Phosphorylation and Truncation of Tau to the Etiopathogenesis of Alzheimer's Disease, Front. Aging Neurosci. 10 (2018) 27, https://doi.org/10.3389/fnagi.2018.00027.

[46] H. Braak, E. Braak, I. Grundke-Iqbal, K. Iqbal, Occurrence of neuropil threads in the senile human brain and in Alzheimer's disease: A third location of paired helical filaments outside of neurofibrillary tangles and neuritic plaques, Neurosci. Lett. 65 (3) (1986) 351–355, https://doi.org/10.1016/0304-3940(86)90288-0.

[47] P. Carneiro, S. Morais, M.C. Pereira, Nanomaterials towards Biosensing of Alzheimer's Disease Biomarkers, Nanomaterials. 9 (2019) 1663, https://doi.org/10.3390/nano9121663.

[48] V. Serafín, M. Gamella, M. Pedrero, A. Montero-Calle, C.A. Razzino, P. Yáñez-Sedeño, R. Barderas, S. Campuzano, J.M. Pingarrón, Enlightening the advancements in electrochemical bioanalysis for the diagnosis of Alzheimer's disease and other neurodegenerative disorders, J. Pharmaceut. Biomed. 189 (2020) 113437, https://doi.org/10.1016/j.jpba.2020.113437.

[49] L.C. Brazaca, I. Sampaio, V. Zucolotto, B.C. Janegitz, Applications of biosensors in Alzheimer's disease diagnosis, Talanta 210 (2020) 120644, https://doi.org/10.1016/j.talanta.2019.120644.

[50] C. Toyos-Rodríguez, J. Calleja-García, L. Torres-Sánchez, A. López, A.M. Abu-Dief, A. Costa, L. Elbaile, R.D. Crespo, J.S. Garitaonandia, E. Lastra, J.A. García, F. J. García-Alonso, A Simple and Reliable Synthesis of Superparamagnetic Magnetite Nanoparticles by Thermal Decomposition of Fe(acac) $_3$, Journal of Nanomaterials. 2019 (2019) 1–10, https://doi.org/10.1155/2019/2464010.

[51] J. Turkevich, P.C. Stevenson, J. Hillier, A study of the nucleation and growth processes in the synthesis of colloidal gold, Discuss. Faraday Soc. 11 (1951) 55–75, https://doi.org/10.1039/df9511100055.
[52] M.-d. Costa, A.d. la Escosura-Muñiz, A. Merkoçi, Electrochemical quantification of gold nanoparticles based on their catalytic properties toward hydrogen formation: Application in magnetoimmunoassays, Electrochem. Commun. 12 (11) (2010) 1501–1504, https://doi.org/10.1016/j.elecom.2010.08.018.
[53] A. de la Escosura-Muñiz, C. Sánchez-Espinel, B. Díaz-Freitas, Á. González-Fernández, M. Maltez-da Costa, A. Merkoçi, Rapid Identification and Quantification of Tumor Cells Using an Electrocatalytic Method Based on Gold Nanoparticles, Anal. Chem. 81 (24) (2009) 10268–10274, https://doi.org/10.1021/ac902087k.
[54] W. Szczerba, J. Żukrowski, M. Przybylski, M. Sikora, O. Safonova, A. Shmeliov, V. Nicolosi, M. Schneider, T. Granath, M. Oppmann, M. Straßer, K. Mandel, Pushing up the magnetisation values for iron oxide nanoparticles via zinc doping: X-ray studies on the particle's sub-nano structure of different synthesis routes, Phys. Chem. Chem. Phys. 18 (36) (2016) 25221–25229, https://doi.org/10.1039/C6CP04221J.
[55] M. Rivero, A. del Campo, Á. Mayoral, E. Mazario, J. Sánchez-Marcos, A. Muñoz-Bonilla, Synthesis and structural characterization of ZnxFe3−xO4 ferrite nanoparticles obtained by an electrochemical method, RSC Adv. 6 (46) (2016) 40067–40076, https://doi.org/10.1039/C6RA04145K.
[56] M. Jouyandeh, J.A. Ali, M. Aghazadeh, K. Formela, M.R. Saeb, Z. Ranjbar, M. R. Ganjali, Curing epoxy with electrochemically synthesized Zn Fe3-O4 magnetic nanoparticles, Prog. Org. Coat. 136 (2019) 105246, https://doi.org/10.1016/j.porgcoat.2019.105246.
[57] A. Ali, H. Zafar, M. Zia, I. ul Haq, A.R. Phull, J.S. Ali, A. Hussain, Synthesis, characterization, applications, and challenges of iron oxide nanoparticles, NSA. Volume 9 (2016) 49–67. https://doi.org/10.2147/NSA.S99986.
[58] J. Mosafer, K. Abnous, M. Tafaghodi, H. Jafarzadeh, M. Ramezani, Preparation and characterization of uniform-sized PLGA nanospheres encapsulated with oleic acid-coated magnetic-Fe 3 O 4 nanoparticles for simultaneous diagnostic and therapeutic applications, Colloids Surf., A 514 (2017) 146–154, https://doi.org/10.1016/j.colsurfa.2016.11.056.
[59] X. Liu, M.D. Kaminski, H. Chen, M. Torno, L. Taylor, A.J. Rosengart, Synthesis and characterization of highly-magnetic biodegradable poly(d, l-lactide-co-glycolide) nanospheres, J. Control. Release 119 (1) (2007) 52–58, https://doi.org/10.1016/j.jconrel.2006.11.031.
[60] R. Singh, P. Kesharwani, N.K. Mehra, S. Singh, S. Banerjee, N.K. Jain, Development and characterization of folate anchored Saquinavir entrapped PLGA nanoparticles for anti-tumor activity, Drug Dev Ind Pharm. 41 (11) (2015) 1888–1901.
[61] F. Mohamed, C.F. van der Walle, Engineering Biodegradable Polyester Particles With Specific Drug Targeting and Drug Release Properties, J. Pharm. Sci. 97 (1) (2008) 71–87, https://doi.org/10.1002/jps.21082.
[62] Y. Zhang, M. García-Gabilondo, A. Rosell, A. Roig, MRI/Photoluminescence Dual-Modal Imaging Magnetic PLGA Nanocapsules for Theranostics, Pharmaceutics. 17 (2020) 16.
[63] J. Ghitman, E.I. Biru, R. Stan, H. Iovu, Review of hybrid PLGA nanoparticles: Future of smart drug delivery and theranostics medicine, Mater. Des. 193 (2020) 108805, https://doi.org/10.1016/j.matdes.2020.108805.
[64] S. Nimesh, in: Gene Therapy, Elsevier, 2013, pp. 197–223, https://doi.org/10.1533/9781908818645.197.
[65] C. Olbrich, U. Bakowsky, C.-M. Lehr, R.H. Müller, C. Kneuer, Cationic solid-lipid nanoparticles can efficiently bind and transfect plasmid DNA, J. Control. Release 77 (3) (2001) 345–355, https://doi.org/10.1016/S0168-3659(01)00506-5.
[66] Surf. Interface Anal. (2002) 5.
[67] I. Migneault, C. Dartiguenave, M.J. Bertrand, K.C. Waldron, Glutaraldehyde: behavior in aqueous solution, reaction with proteins, and application to enzyme crosslinking, Biotechniques 37 (2004) 12.
[68] G.W. Lu, P. Gao, in: Handbook of Non-Invasive Drug Delivery Systems, Elsevier, 2010, pp. 59–94, https://doi.org/10.1016/B978-0-8155-2025-2.10003-4.
[69] I. Barinaga-Rementeria Ramírez, L. Ekblad, B. Jergil, Affinity partitioning of biotinylated mixed liposomes: effect of charge on biotin–NeutrAvidin interaction, J. Chromatogr. B Biomed. Sci. Appl. 743 (1-2) (2000) 389–396, https://doi.org/10.1016/S0378-4347(00)00065-7.
[70] J. Coates, Interpretation of Infrared Spectra, A Practical Approach, in: R.A. Meyers (Ed.), Encyclopedia of Analytical Chemistry, John Wiley & Sons, Ltd, Chichester, UK, 2006: p. a5606. https://doi.org/10.1002/9780470027318.a5606.
[71] F. Wang, P. Liu, T. Nie, H. Wei, Z. Cui, Characterization of a Polyamine Microsphere and Its Adsorption for Protein, IJMS. 14 (2012) 17–29, https://doi.org/10.3390/ijms14010017.
[72] W. Wu, Q. He, C. Jiang, Magnetic Iron Oxide Nanoparticles: Synthesis and Surface Functionalization Strategies, Nanoscale Res Lett. 3 (2008) 397–415, https://doi.org/10.1007/s11671-008-9174-9.
[73] T.D. Tran, M.T.T. Nguyen, H.V. Le, D.N. Nguyen, A. Truong, P.D. Tran, Gold nanoparticle as an outstanding catalyst for the hydrogen evolution reaction, Chem. Commun. 54 (2018) 3363–3366, https://doi.org/10.1039/C8CC00038G.
[74] M. Espinoza-Castañeda, A. de la Escosura-Muñiz, G. González-Ortiz, S.M. Martín-Orúe, J.F. Pérez, A. Merkoçi, Casein modified gold nanoparticles for future theranostic applications, Biosens. Bioelectron. 40 (1) (2013) 271–276, https://doi.org/10.1016/j.bios.2012.07.042.
[75] M.P. Pase, A.S. Beiser, J.J. Himali, C.L. Satizabal, H.J. Aparicio, C. DeCarli, G. Chêne, C. Dufouil, S. Seshadri, Assessment of Plasma Total Tau Level as a Predictive Biomarker for Dementia and Related Endophenotypes, JAMA Neurol. 76 (5) (2019) 598, https://doi.org/10.1001/jamaneurol.2018.4666.
[76] M.A. Sugarman, H. Zetterberg, K. Blennow, Y. Tripodis, A.C. McKee, T.D. Stein, B. Martin, J.N. Palmisano, E.G. Steinberg, I. Simkin, A.E. Budson, R. Killiany, M. K. O'Connor, R. Au, W.W.Q. Qiu, L.E. Goldstein, N.W. Kowall, J. Mez, R.A. Stern, M.L. Alosco, A longitudinal examination of plasma neurofilament light and total tau for the clinical detection and monitoring of Alzheimer's disease, Neurobiol. Aging 94 (2020) 60–70, https://doi.org/10.1016/j.neurobiolaging.2020.05.011.
[77] T.K. Karikari, T.A. Pascoal, N.J. Ashton, S. Janelidze, A.L. Benedet, J.L. Rodriguez, M. Chamoun, M. Savard, M.S. Kang, J. Therriault, M. Schöll, G. Massarweh, J.-P. Soucy, K. Höglund, G. Brinkmalm, N. Mattsson, S. Palmqvist, S. Gauthier, E. Stomrud, H. Zetterberg, O. Hansson, P. Rosa-Neto, K. Blennow, Blood phosphorylated tau 181 as a biomarker for Alzheimer's disease: a diagnostic performance and prediction modelling study using data from four prospective cohorts, The Lancet Neurology. 19 (5) (2020) 422–433, https://doi.org/10.1016/S1474-4422(20)30071-5.
[78] S. Janelidze, E. Stomrud, R. Smith, S. Palmqvist, N. Mattsson, D.C. Airey, N. K. Proctor, X. Chai, S. Shcherbinin, J.R. Sims, G. Triana-Baltzer, C. Theunis, R. Slemmon, M. Mercken, H. Kolb, J.L. Dage, O. Hansson, Cerebrospinal fluid p-tau217 performs better than p-tau181 as a biomarker of Alzheimer's disease, Nat Commun. 11 (2020) 1683, https://doi.org/10.1038/s41467-020-15436-0.
[79] E.H. Thijssen, R. La Joie, A. Strom, C. Fonseca, L. Iaccarino, A. Wolf, S. Spina, I. E. Allen, Y. Cobigo, H. Heuer, L. VandeVrede, N.K. Proctor, A.L. Lago, S. Baker, R. Sivasankaran, A. Kieloch, A. Kinhikar, L. Yu, M.-A. Valentin, A. Jeromin, H. Zetterberg, O. Hansson, N. Mattsson-Carlgren, D. Graham, K. Blennow, J. H. Kramer, L.T. Grinberg, W.W. Seeley, H. Rosen, B.F. Boeve, B.L. Miller, C. E. Teunissen, G.D. Rabinovici, J.C. Rojas, J.L. Dage, A.L. Boxer, Plasma phosphorylated tau 217 and phosphorylated tau 181 as biomarkers in Alzheimer's disease and frontotemporal lobar degeneration: a retrospective diagnostic performance study, The Lancet Neurology. 20 (9) (2021) 739–752, https://doi.org/10.1016/S1474-4422(21)00214-3.